Function of floral fragrance-related microRNAs and their targets in Hedychium coronarium

Fang wang
South China Agricultural University
Liang Liu
South China Agricultural University
Rangcai Yu
South China Agricultural University
Xin Li
South China Agricultural University
Yunyi Yu
South China Agricultural University
Xinyue Li
South China Agricultural University
Yuechong Yue
South China Agricultural University
Yanping Fan
fanyanping@scau.edu.cn

South China Agricultural University

Research Article

Keywords: H. coronarium, miRNAs, Floral fragrance compounds, degradome sequencing

Posted Date: September 13th, 2024

DOI: https://doi.org/10.21203/rs.3.rs-4924260/v1

Additional Declarations: No competing interests reported.

Version of Record: A version of this preprint was published at BMC Genomics on April 30th, 2025. See the published version at https://doi.org/10.1186/s12864-025-11583-0.

Abstract

Background Hedychium coronarium

is highly valued for its intense fragrance, which may be influenced by the expression of microRNAs (miRNAs). miRNAs are a class of small RNAs that play conserved and pivotal regulatory roles throughout plant growth and development, modulating various aspects of plant metabolism. However, the specific functions of miRNAs in the growth and development of *H. coronarium* remain largely unexplored.

Results

Therefore, to identify miRNAs in *H. coronarium* and evaluate their relationship with the synthesis of floral fragrance compounds, we analyzed the volatile compounds and the miRNA patterns at three developmental stages (F1, F5, F9). Our results showed that the volatile emissions of major floral compounds (eucalyptol, ocimene, and linalool) increased with the flower development. Using small RNA sequencing, 171 conserved miRNAs from 24 miRNA families and 32 novel miRNAs were identified. Degradome sequencing revealed 102 mRNA degradation sites corresponding to 90 target genes from 30 miRNA families. The qRT-PCR results indicated that the expression levels of hco-miR393a and hco-miR167n were consistent with the release pattern of floral fragrance compounds, whereas the expression levels of *HcTIR1* and *HcARF8* were inversely correlated with hco-miR393a and hco-miR167n expression. Tobacco co-transformation demonstrated that *HcTIR1* and *HcARF8* are respective targets of hco-miR393a and hco-miR167n. Additionally, treatments with exogenous IAA and the auxin inhibitor PCIB affected both the release of floral fragrance compounds in *H. coronarium* and the expression of hco-miR393a and hco-miR167n. STTM and VIGS experiments indicated that hco-miR167n and hco-miR393a positively regulate the metabolism of floral fragrance compounds, while *HcARF8* and *HcTIR1* act as negative regulators. Dual-luciferase and yeast one-hybrid assays demonstrated that *HcARF8* binds to the promoter of the terpene synthase gene *HcTPS8*, thereby regulating the synthesis of fragrance compounds.

Conclusions

This is the first report to identify miRNAs in *H. coronarium* and elucidate their expression profiles in petal tissues across different developmental stages. These findings provide new insights into the molecular regulation of floral fragrance compound synthesis and underscore the role of miRNAs in the Zingiberaceae family of plants.

Background

The study of gene expression and its regulatory mechanisms is crucial for understanding plant growth and development. Small RNAs (sRNAs) play significant roles in regulating plant metabolism, hormone responses, and responses to various stresses [1]. Among them, microRNA (miRNAs) play important regulatory roles post-transcriptionally in eukaryotic organisms [2]. miRNAs are a class of conserved endogenous sRNAs in plants and animals, typically 18–25 nucleotides in length. They regulate the expression of target genes/mRNAs post-transcriptionally in a sequence-specific manner, usually negatively affecting mRNA accumulation [3]. Extensive research has demonstrated that miRNAs play roles in plant growth, development, hormone signaling, and responses to environmental stresses. For instance, in rice, OsmiR396d targets the *OsGRF6* gene, participating in gibberellin biosynthesis and signaling, thereby controlling plant height [4]. In Papaya, cpa-miR390a targets *CpARF19*, participating in ethylene and auxin signaling pathways, thus influencing papaya ripening [5]. In *Arabidopsis thaliana*, miR160 regulates hypocotyl elongation by downregulating ARF genes [6], while miR319 promotes cell proliferation by negatively regulating TCP4 [7]. However, miRNAs in *Hedychium coronarium* remain poorly understood to date. Therefore, it is essential to investigate miRNAs and their targets in *H. coronarium*.

Furthermore, extensive research indicates that miRNAs play a crucial role in regulating the expression of genes related to flower development in plants. For example, miR397 modulates flowering time through the targeted regulation of the LAC15 gene [8]. miR156 and miR157 prevent early flowering by inhibiting the translation of the SPL3 gene [9]. miR159 alters flower color and the formation of floral meristems by targeting MYB transcription factors in the GA pathway [10]. miR172 controls the size of floral meristems by regulating the expression of AP2 genes [11]. miR164 regulates the number of petals by targeting the CUC1 and CUC2 genes, which encode NAC domain proteins[12]. Studies on miRNAs in horticultural plants have primarily focused on the regulation of floral organ development, but there is limited information on miRNAs in aromatic plants, which restricts the breeding of fragrant plants.

Currently, with the development of high-throughput sequencing technology, a new method for detecting miRNA targets, known as degradome sequencing, has emerged. This technique combines the advantages of high-throughput deep sequencing and bioinformatics analysis. In this method, deep sequencing analysis is performed on the degraded fragments of target mRNAs cleaved by miRNAs to identify miRNA targets[13]. This approach has already been successfully applied to the study of miRNA targets in *Arabidopsis*[14], rice[15], and maize[16]. Kim et al.[17] conducted sRNA sequencing on *Rosa* and identified 267 miRNAs, including 25 novel miRNAs and 242 conserved miRNAs, which play important roles in the flower development and phenotypes of roses. Jin et al.[18] performed sRNA sequencing on peony (*Paeonia ostii*) flower buds, discovering 12 conserved miRNAs and 18 novel miRNAs that are involved in the response to copper stress.

miRNA-mediated regulation of auxin homeostasis is a highly conserved process. Several major miRNA gene families are involved in determining the balance of auxin concentration and signaling, including miR160, miR167, miR393, and miR847, which play roles in plant growth, development, and stress responses. Among these, miR160 and miR167 target auxin response factors (ARFs), thereby regulating

the expression of downstream auxin-responsive genes related to plant development and stress responses[19]. MiR393 targets auxin receptors, transport inhibitor response 1 (TIR1), and auxin signaling F-box (AFB) proteins, modulating growth, development, and stress responses in various plant species[20]. While the crucial role of miRNAs in auxin signaling pathways is well established, it remains unclear whether miRNAs are involved in auxin signal transduction and the synthesis of fragrance compounds in *H. coronarium*. The potential mechanisms by which auxin signaling cascades regulate *H. coronarium* fragrance still need to be explored.

H. coronarium is a perennial herbaceous plant belonging to the Zingiberaceae family. It is known for its beautiful flower shape and strong fragrance, making it widely used in horticultural breeding and the fresh-cut flower market, with significant economic and ecological value. Currently, research on the regulatory mechanisms of *H. coronarium* flower fragrance is substantial, with particular emphasis on terpene synthase studies. Specifically, both *HcTPS5* and *HcTPS8* catalyze the production of linalool from GPP, whereas *HcTPS7* predominantly converts GPP into sabinene[21, 22]. However, the regulatory mechanisms of miRNAs in the growth, development, and synthesis of fragrance compounds in *H. coronarium* remain unclear. This lack of understanding significantly limits the progress of breeding improvement. Therefore, the identification and analysis of miRNAs, prediction of their target genes, and elucidation of their mechanisms of action will become new directions in *H. coronarium* research. This study is the first to use high-throughput sRNA sequencing technology to identify miRNAs at different developmental stages of *H. coronarium*. Combining GC-MS, degradome sequencing, and bioinformatics analysis, we predicted the target genes of miRNAs and identified miRNAs related to fragrance. Molecular biology techniques were used to validate the functions of these miRNA target genes and the molecular mechanisms regulating fragrance, providing a theoretical basis for transcriptional regulation in the synthesis of aromatic compounds in *H. coronarium*.

Materials and methods

Plant material

The tested plant is *H. coronarium*, which is planted in the nursery of Flower Research Center of South China Agricultural University. Based on the flowering stage of *H. coronarium*, six stages (F1 ~ F6) were identified (Fig. 1). Petals from the budding stage (F1), full blooming stage (F5), and senescence stage (F6) were collected as experimental materials, then frozen in liquid nitrogen, and stored in refrigerator at -80 ℃.

Identification of volatile aroma compounds in H. coronarium

Three flowers from the same period of *H. coronarium* were weighed and placed in a clean glass bottle. A total of 2 μL of ethyl anthranilate was added as an internal standard, and the bottle was sealed and allowed to react for 15 minutes. A high-temperature activated extraction needle (SPEM, 50/30 μm, DVB/CAR/PDMS) from the GC-MS instrument was then inserted into the glass bottle for headspace

extraction for 15 minutes. Afterward, the extraction needle was inserted into the GC-MS inlet for injection, and removed the needle once the injection was complete. All samples were analyzed using an Agilent 7890A gas chromatograph coupled with a 5975C mass spectrometer. The chromatographic column used was an Agilent DB-5MS capillary column (122–5532; 30 m; I.D: 0.25 mm; film: 0.25μm). The operating parameters were set as follows: injection port temperature of 250℃ with no split, a column head pressure of 50 Pa, and a flow rate of 1 mL/min; sampling time ranged from 3 to 5 minutes. The oven temperature was initially held at 40℃ for 2 minutes, then ramped from 40℃ to 250℃ at a rate of 10 ℃/min, and held at 250℃ for 5 minutes. The temperatures of the mass spectrometer ion source and the ion source surface were maintained at 230℃ and 280℃, respectively; electron impact ionization was set at 50–550 amu. Gas chromatography separates volatile components, with different components forming their respective chromatographic peaks. The mass spectrometer qualitatively identifies different component substances, and the mass spectra of each component are analyzed using the NIST2008 library to determine the chemical composition of volatile substances in different samples. Quantitative analysis is performed using a relative quantification method.

RNA extraction and sequencing of small RNA

Petals from stages F1, F5, and F6 were sampled, and RNA was extracted following the HiPure Plant RNA Mini Kit (Magen, Guangzhou, China) protocol, with three replicates for each treatment. RNA samples were then assessed for purity, concentration, and integrity using Nanodrop to ensure the use of qualified samples for sequencing. RNA samples meeting purity standards were sent to Novogene Company (Beijing, China) for library construction and Illumina sequencing. Small RNA libraries of F1, F5, and F6 were constructed. After removing low-quality reads, clean reads were aligned and classified against the Silva database, GtRNAdb database, Rfam database, and Repbase database using Bowtie software for sequence alignment and annotation. Non-coding RNAs such as ribosomal RNA, transfer RNA, nuclear small RNA, and repetitive sequences were removed to obtain Unannotated reads.

Prediction of miRNA target genes

Three qualitative degradome libraries were constructed to identify miRNA target transcripts. Align the filtered Unannotated reads with miRNAs from all species in the miRBase 22.1 database to identify known miRNAs in *H. coronarium*. Employ miRDeep2 and Mfold software for structure prediction of unannotated miRNAs and precursor sequences, thereby obtaining new miRNAs. Predict target genes for both known and new miRNAs using psRNATarget. Utilize BLAST software to align predicted target gene sequences with the GO, KEGG, and Rfam databases to obtain functional annotation information for target genes.

RT-qPCR expression analysis of target genes

The design of miRNA target gene forward and reverse primers was carried out using Premier 5.0 software, followed by amplification using the ABI7500 fluorescence quantitative PCR system with a reaction volume of 20 μL. The reaction mixture consisted of 2 μL cDNA template, 10 μL of Hieff® qPCR

SYBR Green Master Mix (Yeasen Biotechnology, Shanghai, China), 7.2 μL of RNase-free H_2O and 0.4 μL of each forward and reverse primer. The RPS gene was chosen as an internal control for normalizing the expression data of target genes. The qRT-PCR program consisted of an initial denaturation step at 95℃ for 30 s, followed by denaturation at 95℃ for 5 s, annealing at 55℃ for 30 s, and extension at 72℃ for 30 s, repeated for 40 cycles. The melting curve program started at 60℃ and increased at a rate of 1% to 95℃. The relative expression levels between different treatments were calculated using the $2^{-\triangle\triangle Ct}$ method.

Transient expression analysis

The interaction between miRNAs and their target gene was confirmed in vivo using a transient expression system. PMS4-*ARF8*/*TIR1* and pOx-hco-miR167n/miR393a overexpression vectors were constructed respectively. Co-expression of miRNAs and their targets in *N. Benthamiana* leaves using *Agrobacterium tumefaciens* EHA105 infiltration. After 3 days of infiltration, the GFP fluorescence of leaves was observed by laser scanning confocal microscope (Zeiss LSM800).

Effects of exogenous IAA and auxin inhibitor PCIB on fragrance compounds and related genes

Several flower branches at the bud break stage were selected and individually placed in conical flasks containing sterile water (blank control), 0.1 mM IAA, and 350 mg/L PCIB, respectively. These flasks were then positioned in an artificial growth chamber with a 12-hour photoperiod for cultivation. Following this, petals were harvested for the analysis of volatile fragrance compounds using GC-MS, and the expression of related genes was detected by RT-qPCR.

The interaction between miRNA and target gene

To validate the relationship between miRNAs and their target genes, we conducted short tandem target mimic (STTM) and barley stripe mosaic virus-mediated (BSMV) virus-induced gene silencing (VIGS) experiments, in which we constructed pOx-STTM-miR167n/miR393a vectors and VIGS-*ARF8*/*TIR1* constructs, respectively. The constructed vectors were transformed into *A. tumefaciens* EHA105, which was then used to infiltrate *H. coronarium*. After a 24-hour incubation period, the content of volatile fragrance compounds was measured, followed by an analysis of the expression levels of genes related to aroma synthesis.

Dual-luciferase assay

The full-length coding sequence of *HcARF8* was amplified and inserted into the pGreen II 0029 62-SK vector and the promoters of *HcTPS3*, *HcTPS5*, and *HcTPS8* were constructed in the pGreen II 0800-LUC vector. Primers used for vector construction are listed in Supplemental Table S1. All constructs were confirmed by sequencing and transferred into *Agrobacterium tumefaciens* (GV3101) by heat shock. Determination of Dual-luciferase assay in *N. benthamiana* leaves was performed by reference method. After 4 days, the Dual Luciferase Reporter Gene Assay Kit (RG027, Beyotime) was used to measure the fluorescence values of firefly luciferase (LUC) and renilla luciferase (REN), with readings taken using the

Thermo Scientific Luminoskan Ascent instrument (Gelview 6000Pro II, China). Finally, the relative ratio of LUC/REN was calculated.

Yeast one-hybrid (Y1H) assay

The Matchmaker Gold Yeast One-Hybrid Library Screening System (Clontech) was used to test the interaction of *HcARF8* with the *HcTPS3*, *HcTPS5*, and *HcTPS8* promoter. The promoter fragment of *HcTPS3*, *HcTPS5*, and *HcTPS8* were inserted into pAbAi vector and the CDS of *HcARF8* was inserted into pGADT7 vector. The recombinant *HcTPS3*, *HcTPS5*, and *HcTPS8* promoter-pAbAi vector was linearized and transformed into the Y1HGold yeast strain to test the promoter autoactivation. The combination of pGADT7-*HcARF8* and the pAbAi-*HcTPS3/HcTPS5/HcTPS8pro* was transformed together into Y1HGold. Additionally, combinations of the empty vector pGADT7 and *HcTPS3*/*HcTPS5*/*HcTPS8* promoter were co-transformed into Y1HGold as negative controls. The primers for vector construction are listed in Supplemental Table S1.

Statistical analysis

Data were organized using Microsoft Excel software (Version, 2019) and SPSS 26.0 software. All data are represented as mean ± standard deviation (SD). Statistical significance was determined using Duncan's test and Student's t-test.

Results

Changes of volatile compounds in H. coronarium during different developmental stages

Volatile aroma compounds were measured in the flowers of *H. coronarium* at the F1, F5, and F6 periods (Fig. 2). Ocimene, linalool, and eucalyptol were identified as the main aroma compounds. The concentrations of these compounds increased continuously as the flowers developed, reaching the highest levels at the full blooming stage (F5).

Overview of high-throughput small RNA sequencing from H. coronarium

Small RNA libraries were constructed from petals of *H. coronarium* at three stages, F1, F5, and F6. For each library, on average, more than 12 million clean reads and over 2.5 million unique reads were obtained (Table S2). The lengths of small RNA sequences from *H. coronarium* were mainly concentrated at 18–30 nt, with the highest number of miRNAs distributed at 23–24 nt in length, which is consistent with the results of miRNA studies of other plant species (Fig. S1).

Screening and analysis of differentially expressed miRNAs in H. coronarium

The miRNAs from the three stages of F1, F5, and F6 were compared using DESeq2-EBseq software to screen the differentially expressed miRNAs with conditions set at p-value < 0.05 and $|\log_2(\text{foldchange})| > 1$. As illustrated in Fig. 3, a total of 122 differentially expressed miRNAs were identified across these three stages. Specifically, in the comparison between F5 and F1, 11 miRNAs were upregulated and 7

were downregulated; for F6 versus F1, 51 miRNAs showed upregulation while 42 were downregulated; in the contrast between F6 and F5, 43 miRNAs were upregulated and 35 downregulated. Interestingly, as the flowers developed, the number of up-regulated miRNAs was significantly higher than that of down-regulated miRNAs from F1 to F6. Notably, miR162 was found to be differentially expressed in all three pairwise comparisons (Fig. 3).

Identification of known miRNAs and prediction of novel miRNAs

To identify conserved miRNAs in *H. coronarium*, the unannotated clean reads obtained from sequencing were compared with the conserved miRNAs of known plants in miRbase (version 22.1). A total of 171 known miRNAs were identified in *H. coronarium* belonging to 24 conserved miRNA families (Table S3). Among them, miR396, miR167, miR156, miR166, miR171, miR159, and miR168 contain half of the members. miR396 was the largest family, with 22 members, followed by miR167 and miR156, with 19 and 16 members, respectively (Fig. S2). The composition of bases in miRNA sequences is closely related to their biological properties and secondary structure features. By statistically analyzing the distribution pattern and probability of each base of known miRNAs, it can be seen from Fig. S3 that there is a significant difference in the chances of random assignment of the four bases A, C, G, and U in the sequences of known miRNAs. Across the 22 different positions of the known miRNA sequences, the bases with the greatest probability of occurrence in the stages of F1, F5, and F6 are the bases of U, U, and G, respectively, accounting for 28.98%, 29.87%, and 30.38%. Conversely, the bases with the lowest probability of occurrence in all three stages were C bases, accounting for 20.60%, 16.45%, and 17.72%, respectively. Further analysis of miRNA sequences with varying lengths (Fig. S3) reveals a striking bias towards U as the initial base in samples from F1, F5, and F6 stages, with proportions reaching 59.35%, 54.80%, and 49.55%, respectively. This underscores a marked preference for U at both specific sequence locations and as the leading nucleotide in miRNA sequences during these developmental stages.

After identifying known miRNAs, the novel miRNAs were predicted using miREvo and mirdeep2 prediction software, resulting in the identification of 32 novel miRNAs (Table 1). The novel miRNAs are mapped to their respective positions on the *H. coronarium* chromosomes, as shown in Supplementary Fig. S4.

Table 1
Novel miRNA sequence information of *H. coronarium*

Novel miRNAs	Sequences	Length	Chr_ID
miRn1	TCAAGCTGTCAGCATGATCTGA	22	000028F_arrow_pilon
miRn2	GGCAAGTCGTTTTTGGCTAGA	21	000040F_arrow_pilon
miRn3	TTTTGGCGTGGTCTCATTAAG	21	000212F_arrow_pilon
miRn4	TCGAGGAAGATGAGTAGGTGG	21	000371F_arrow_pilon
miRn5	CTTCAGATCTGTGCATGTACAC	22	002454F_arrow_pilon
miRn6	TTCCGTATGTGCTTGCAGAAG	21	Hic_asm_0
miRn7	TGGGCTCAAAAGGATAAAGATA	22	Hic_asm_0
miRn8	AACGTATAACTACTGACTTAT	21	Hic_asm_1
miRn9	TCATGTGGGCTCTGACCGCGC	21	Hic_asm_1
miRn10	TTATGGTGCTACTGAATGAGC	21	Hic_asm_1
miRn11	TTGTGGTGCTATTGAATGAGC	21	Hic_asm_1
miRn12	TTGTGGTGCTATTGAATGAGC	21	Hic_asm_1
miRn13	CTTCTGATCTGTGCATGTACAC	22	Hic_asm_10
miRn14	GGCAGATGTAGCCAAGTGGA	20	Hic_asm_11
miRn15	ACTGACTGAGAGCTCTTTCACG	22	Hic_asm_11
miRn16	TTTGATCTTCTGAAGTGCAGG	21	Hic_asm_11
miRn17	ACCGATCGTTTCGAGAAGAGC	21	Hic_asm_11
miRn18	ACCGATCGTTTCGAGAAGAGC	21	Hic_asm_11
miRn19	CGGAGGCGGTGATGGCCGGGGG	22	Hic_asm_11
miRn20	TCATGTCATTCCGATCTCTCT	21	Hic_asm_12
miRn21	CTTTGTGTTGGAGATATTCTTC	22	Hic_asm_13
miRn22	TTTCGTCGCTAAATTTGATGT	21	Hic_asm_14
miRn23	GGCGGGTTGCGAGCTCTTATG	21	Hic_asm_16
miRn24	ATGGCTAGGGACTGGGGGTCT	21	Hic_asm_16
miRn25	CTTCAGATCTGTGCATGTACAC	22	Hic_asm_16
miRn26	TGTGTTGCCTGGGAATTTTGCC	22	Hic_asm_2
miRn27	TATATGGTTGGTGGATCATGA	21	Hic_asm_3

Novel miRNAs	Sequences	Length	Chr_ID
miRn28	TACGTGTTCGTCTAGTTCTCT	21	Hic_asm_4
miRn29	GAGGTCTGTAATTTGATACTGC	22	Hic_asm_5
miRn30	TTTGCATAACTCAGGAGCTGC	21	Hic_asm_9
miRn31	GTGTAGTTTTCCTTTGGCAGG	21	Hic_asm_9
miRn32	TGAGATCATCGATTGCTGGAGA	22	Hic_asm_9

Target prediction of miRNAs using degradome sequencing

To further investigate the regulatory roles of miRNAs, degradome sequencing was performed on petals from three stages: F1, F5, and F6. After discarding low-quality reads and adapter sequences, we obtained 26,333,976 clean reads. Using the TargetFinder target gene prediction software, the miRNAs obtained from high-throughput sequencing of the *H. coronarium* transcriptome database were subjected to target gene prediction (Table S4). For the identification of cleavage sites, the targets were grouped into four categories according to the relative abundance of degradome reads mapping at the predicted miRNA target site relative to the abundance of the reads located at other sites. Representative target plots of identified miRNA targets are shown in (Fig. S5). In Category 0, the peak value of tags was found at the predicted cleavage site of miRNA and there was only one maximum on the transcript. If the abundance of tags was between the median and the maximum, it was grouped as Category 2 or Category 3. In Category 4, the abundance of tags was equal to, or less than the median.

Additionally, a total of 102 miRNA cleavage sites corresponding to 90 target genes across 30 miRNA families were identified, among which 80 target genes were successfully annotated (Table 2), and these targets were predominantly transcription factors. Previous studies have demonstrated that one miRNA can target multiple target genes, and conversely, one target gene can also be targeted by multiple miRNAs. In our study, hco-miR159 had the largest number of predicted target genes, with 10 target genes identified, followed by hco-miR396 (8 target genes), and hco-miR156 (7 target genes). Furthermore, through GO and KEGG enrichment analysis of the target genes, it was found that these target genes are predominantly enriched in the plant hormone signal transduction pathway (Fig. S6).

Table 2
Targets of *H. coronarium* miRNA identified by degradome sequencing

miRNA family	Target gene ID	Putative function
hco-miR156	comp46181_c0	callose synthase 3-like
	comp48189_c0	squamosa promoter-binding-like protein 16
	comp30142_c0	unknown
	comp27366_c0	homeobox-leucine zipper protein HOX16-like
	comp37992_c0	ATP-dependent zinc metalloprotease FTSH 2
	comp41926_c0	heptahelical transmembrane protein ADIPOR3-like
	comp48430_c0	ADP-ribosylation factor 1
hco-miR159	comp31174_c0	proteasome subunit beta type-5-like
	comp31186_c0	unknown
	comp47835_c0	transcription factor GA*MYB*-like
	comp47107_c0	uncharacterized LOC103983792
	comp49067_c0	protein plastid movement impaired 1-related 1
	comp35557_c0	FHA domain-containing protein FHA2-like
	comp40668_c0	protein DEK
	comp40625_c0	unknown
	comp46428_c0	heparanase-like protein 2
	comp43947_c0	glyoxysomal fatty acid beta-oxidation multifunctional protein MFP-a-like
hco-miR162	comp45610_c0	endoribonuclease Dicer homolog 1
hco-miR166	comp43255_c0	homeobox-leucine zipper protein HOX9
	comp42585_c0	serine/threonine-protein kinase STY46-like
	comp48810_c0	homeobox-leucine zipper protein HOX32-like
hco-miR167	comp47235_c0	uncharacterized LOC105049210
	comp45490_c0	auxin response factor 8-like ARF8
	comp42823_c0	unknown
	comp40432_c0	UDP-galactose transporter 1
	comp17573_c0	mitochondrial-processing peptidase subunit alpha-like

miRNA family	Target gene ID	Putative function
	comp96039_c0	unknown
hco-miR168	comp45501_c1	uncharacterized LOC109839632
hco-miR169	comp34201_c0	cystinosin homolog
hco-miR171	comp47960_c0	scarecrow-like protein 27
	comp45596_c0	scarecrow-like protein 15
	comp32225_c0	uncharacterized LOC103931388
	comp47572_c0	cyclin-dependent kinase G-2
hco-miR319	comp29930_c0	transcription factor TCP4
	comp45955_c1	transcription factor PCF5-like
	comp47835_c0	transcription factor GA*MYB*-like
	comp39846_c0	FRIGIDA-like protein 4a
	comp42681_c0	uncharacterized LOC103989154
hco-miR393	comp47036_c1	genome shotgun sequence
	comp44931_c0	protein DEK-like
	comp48815_c0	transport inhibitor response 1-like protein TIR1
	comp47879_c0	cellulose synthase-like protein H1
hco-miR394	comp47147_c0	uncharacterized LOC103984447
	comp48385_c1	F-box only protein 6
	comp48438_c0	phosphoinositide phosphatase SAC3
	comp16691_c0	tRNA (guanine(9)-N1)-methyltransferase
	comp34494_c1	laminin subunit alpha 3 (LAMA3)
	comp40642_c0	signal recognition particle subunit SRP72-like
	comp47501_c0	cyclin-dependent kinase F-3
hco-miR395	comp41552_c0	ATP sulfurylase 1, chloroplastic-like
	comp42239_c1	peroxidase 73
hco-miR396	comp30210_c0	40S ribosomal protein S13
	comp43966_c1	CBL-interacting protein kinase 18-like

miRNA family	Target gene ID	Putative function
	comp46277_c0	DExH-box ATP-dependent RNA helicase DExH10
	comp48706_c0	oligopeptide transporter 7-like
	comp27123_c0	post-GPI attachment to proteins factor 3-like
	comp45123_c0	ABC transporter G family member 31
	comp41841_c0	RPM1-interacting protein 4
	comp68639_c0	alpha-galactosidase 1-like
hco-miR399	comp43073_c0	unknown
hco-miR408	comp36980_c2	whole genome shotgun sequence
	comp41984_c0	basic blue protein-like
hco-miR482	comp32217_c0	unknown
	comp40779_c0	TMV resistance protein N-like
	comp47696_c1	aspartyl protease 25
	comp41519_c0	splicing factor 3B subunit 2
hco-miR5179	comp41070_c0	APETALA3-like protein (AP3)
	comp45682_c0	uncharacterized LOC108953381
	comp48507_c0	AAA-ATPase At4g25835-like
hco-miR528	comp38590_c0	Japonica Group DNA, chromosome 2, cultivar: Nipponbare, complete sequence
	comp49773_c0	protein DMP2-like
hco-miR530	comp44896_c0	ABC transporter F family member 5
hco-miRn1	comp39725_c0	TIP4I-like family protein (TIP4I)
	comp45490_c0	auxin response factor 8-like
hco-miRn11	comp34044_c0	polygalacturonase-like
	comp39121_c1	chromosome Lu8
	comp49145_c0	transformation/transcription domain-associated protein-like
hco-miRn12	comp34044_c0	polygalacturonase-like
	comp39121_c1	chromosome Lu8

miRNA family	Target gene ID	Putative function
	comp49145_c0	transformation/transcription domain-associated protein-like
hco-miRn14	comp28588_c0	unknown
	comp34328_c0	ABC transporter A family member 7-like
	comp48561_c0	spermatogenesis-associated protein 20
hco-miRn15	comp44913_c0	18S ribosomal RNA gene
hco-miRn19	comp38703_c0	acyl-CoA-binding domain-containing protein 3-like
hco-miRn21	comp38688_c0	hypothetical protein
	comp37459_c0	unknown
hco-miRn24	comp36980_c2	whole genome shotgun sequence
hco-miRn31	comp28405_c0	annexin D4-like
	comp45540_c0	activating signal cointegrator 1
hco-miRn32	comp27938_c0	unknown
	comp43835_c0	uncharacterized LOC105051789
hco-miRn4	comp23808_c0	threonine dehydratase biosynthetic, chloroplastic
	comp36577_c0	ASC1-like protein 3
	comp45224_c0	Serine-rich protein

Validation of miRNA and target gene expression in H. coronarium

According to previous studies, the auxin-related signal elements can indirectly regulate the production of volatile compounds in *H. coronarium*. Presently, it is believed that the key signal elements involved in auxin signal transduction are the SCF complex (SKP1-CUL1-TIR1), auxin/ indole-3-acetic acid proteins (Aux/IAAs) and auxin response factor (ARFs) [23]. Combined with the results of miRNA high-throughput sequencing and degradation sequence analysis, it was found that auxin-related signal elements *HcARF8* and *HcTIR1* were paired with hco-miR167n and hco-miR393a, respectively. This suggests that these miRNAs might be involved in the accumulation of volatile fragrance compounds in *H. coronarium* by regulating their respective targets. And the secondary structure predictions for the two miRNAs related to floral fragrance compounds synthesis are shown in Fig. S7.

To preliminarily verify whether hco-miR167n and hco-miR393a are related to the production of volatile compounds in *H. coronarium*, the expression patterns of *HcTIR1*-miR393a and *HcARF8*-miR167n were analyzed by qRT-PCR. The results showed that the expression of hco-miR393a and hco-miR167n was consistent with the release of volatile aroma compounds. Meanwhile, the expression of *HcTIR1* and

HcARF8 was relatively high in the F1 bud stage, remained at a low level throughout the blooming period, and increased slightly in the F6 decline stage (Fig. 4). This suggests that *HcARF8* and *HcTIR1* may be negative regulators of the production of volatile compounds in *H. coronarium*. Conversely, hco-miR167n and hco-miR393a have the opposite expression trend, leading to the preliminary hypothesis that these microRNAs may participate in the formation of volatile compounds by modulating the auxin-related signaling components *HcARF8* and *HcTIR1*. Moreover, it can be seen from Fig. 4 that the expression of miRNA and target genes present opposite expression patterns, which is consistent with the phenomenon of miRNA cutting on target genes.

Additionally, the target relationships between *HcARF8*-miR167n and *HcTIR1*-miR393a were confirmed using a tobacco transient expression system. The transient expression system was constructed to confirm that miRNAs degrade their target genes in vivo. Remarkably, in the experimental groups with pOx-hco-miR167n + PMS4-*HcARF8* and pOx-hco-miR393a + PMS4-*HcTIR1* constructs, only faint fluorescence was observed compared to the negative control groups comprising pOx-hco-miR167n + PMS4, pOx + PMS4-*HcARF8*, pOx-hco-miR393a + PMS4, and pOx + PMS4-*HcTIR1*, which displayed intense fluorescence (Fig. 5). This observation suggests that the miRNAs are effectively degrading their target genes in vivo. In summary, hco-miR393a and hco-miR167n respectively bind to *HcTIR1* and *HcARF8*, leading to mRNA degradation or translational repression. This further validates in vivo that *HcTIR1* and *HcARF8* are the target genes of hco-miR393a and hco-miR167n, respectively.

Changes in volatile fragrance compounds contents and gene expression in H. coronarium after exogenous IAA and PCIB treatments

HcARF8 and *HcTIR1* are two pivotal signaling components in the auxin response pathway, and exogenous applications of IAA and the auxin inhibitor PCIB were found to impact the emission of volatile aroma compounds in *H. coronarium*. The results showed that after 0.1 mM IAA treatment of *H. coronarium*, the contents of ocimene, eucalyptol and allo-ocimene, as well as the expression levels of hco-miR167n and hco-miR393a, significantly increased, whereas methyl benzoate content notably decreased ($p < 0.05$). Conversely, upon treatment with 350 mg/L PCIB, the concentrations of ocimene, linalool, allo-ocimene, and methyl benzoate, as well as the expression of hco-miR167n, hco-miR393a, *HcARF8*, and *HcTIR1*, were all significantly reduced (Fig. 6). These findings suggest that hco-miR167n and hco-miR393a can be regulated by exogenous auxin and further confirm that *HcARF8* and *HcTIR1*, as targets of hco-miR167n and hco-miR393a respectively, indirectly modulate the synthesis and release of aroma compounds in *H. coronarium*.

Functional validation of HcARF8-miR167n and HcTIR1-miR393a in H. coronarium

Short tandem target mimic (STTM) technology is an effective technique for silencing microRNAs (miRNAs) and has been successfully applied in plants [24]. After STTM to interfere with hco-miR167n and hco-miR393a, the flower aroma compounds such as ocimene, linalool, myrcene, and methyl benzoate decreased significantly compared with the control (Fig. 7A). To further analyze the expression changes of related genes after STTM interference with hco-miR167n and hco-miR393a, qRT-PCR was

employed. The results showed that after transient overexpression interfered with hco-miR167n, the expression of *HcARF8* increased, while the expression of terpene synthase genes *HcTPS8*, *HcTPS10*, and methyl benzoate synthase gene *HcBSMT1* decreased significantly compared with the control (Fig. 7B, D). However, after transient overexpression interfered with hco-miR393a, the expression of *HcTIR1* decreased, and the expression of terpene synthase gene *HcTPS3*, *HcTPS5*, and methyl benzoate synthase gene *HcBSMT2* decreased significantly compared with the control (Fig. 7C, D). The results further showed that *HcARF8* and *HcTIR1* were the target genes of hco-miR167n and hco-miR393a respectively, and hco-miR167n and hco-miR393a were positive regulators of flower aroma compounds in *H. coronarium*.

After VIGS *HcARF8*, the contents of linalool and methyl benzoate increased significantly, while the contents of ocimene and eucalyptol decreased significantly. After VIGS *HcTIR1*, the content of linalool increased significantly, while the content of eucalyptol decreased significantly (Fig. 8A). To further analyze the expression changes of related genes after VIGS *HcARF8* and *HcTIR1*, qRT-PCR was employed. The results showed that after silencing *HcARF8*, the expression of terpene synthase gene *HcTPS1*, *HcTPS3*, *HcTPS5* and *HcTPS10* increased significantly, while the expression of methyl benzoate synthase gene *HcBSMT2* decreased significantly compared with the control (Fig. 8B, D). However, after silencing *HcTIR1*, the expression of terpene synthase genes *HcTPS1*, *HcTPS3*, *HcTPS5*, *HcTPS8*, *HcTPS10* and methyl benzoate synthase gene *HcBSMT1* increased significantly (Fig. 8C, D). The above results suggest that *HcARF8* and *HcTIR1* may be negative regulators of flower aroma compounds.

Transcriptional activity analysis of HcARF8 on key genes involved in aroma compounds synthesis

To further elucidate the transcriptional regulation of *HcARF8* on the synthase genes involved in *H. coronarium* aroma compounds synthesis, CaMV35S-*HcARF8* vector and *HcTPS8/HcTPS5/HcTPS8pro*-LUC/CaMV35S-REN vector were constructed and transferred into *A. tumefaciens* (EHA105), respectively. After infecting tobacco leaf cells, the LUC and REN activity were detected. Compared with the CaMV35S-Empty control group, the expression of LUC reporter gene driven by *HcTPS8pro* was significantly enhanced by CaMV35S-*HcARF8* transfer, which was 3.45 times higher than that of the control group (Fig. 9A, B). Moreover, *HcTPS3/5/8pro*-pAbAi vector and *HcARF8*-pGADT7 vector were constructed respectively, and the interaction between *HcARF8* and *HcTPS*3/5/8 promoter was verified by yeast one-hybrid assays. The yeast cells transformed with *HcARF8* along with *HcTPS38pro*-pAbAi were capable of growth on medium containing AbA (300 ng/mL), whereas yeast cells transformed with the empty vector control pGADT7 remained unable to grow on AbA-containing plates (Fig. 9C). Collectively, these findings indicate that the transcription factor *HcARF8* can bind to the promoter of *HcTPS8* and transcriptionally inhibit its expression, thereby participating in the regulation of terpenoid volatile aroma compound biosynthesis in *H. coronarium*.

Discussion

MicroRNA is a non-coding small RNA molecule that regulates gene expression by targeting mRNAs to inhibit the translation of target mRNAs during or after transcription [25]. In recent years, more and more studies have shown that miRNAs are involved in the regulation of plant secondary metabolites. Currently, a variety of miRNAs regulating secondary metabolic biosynthesis have been identified in plants by small RNA and degradome sequencing, such as miR160 [26], miR156 [27], and miR4995 [28]. In *Arabidopsis thaliana*, miR858a targets MYBL2, regulating anthocyanin accumulation by modulating the expression of chalcone synthase (CHS), chalcone isomerase (CHI), and flavanone 3-hydroxylase (F3H) [29]. In *Gerbera hybrida*, Ghy-miRn75 targets the bHLH transporter GMYC1, which binds to the promoter of GMYB10 to activate PGDFR2, thereby regulating anthocyanin biosynthesis [30]. With the continuous development of sequencing technology, bioinformatics algorithms and high-throughput sequencing methods have been widely applied to explore plant miRNAs. In this study, small RNA sequencing was performed on the petals of *H. coronarium* at different developmental stages, 171known miRNAs and 32 specific miRNAs of 24 miRNAs families were identified. Several miRNA families (such as hco-miR156, hco-miR166, hco-miR167, hco-miR408, and hco-miR396) showed high expression levels during stages F1, F5, or F6, which is similar to previous results observed in *Gerbera hybrida* [30] and O*smanthus fragrans* [31]. Additionally, the sRNAs in *H. coronarium* are most abundant at a length of 24 nucleotides, which is consistent with the sRNA length distribution in *Lilium davidii* var. *unicolor* [32] and *Phaseolus vulgaris* L. [33]. However, this distribution differs from that observed in *Canna* [34] and *Brassica juncea* [35], indicating that the sRNA length distribution varies among different plant species.

To elucidate the role of miRNAs in the regulation of *H. coronarium* aroma, it is crucial to analyze miRNAs and their potential target genes. In this study, differentially expressed miRNAs were identified to monitor transcriptional changes in different developmental stages of *H. coronarium*. A total of 122 differentially expressed miRNAs were found across the three comparison groups, in which the number of upregulated miRNAs exceeding that of downregulated miRNAs (Fig. 3). Additionally, these differentially expressed miRNAs exhibited significantly different expression patterns in different developmental stages, indicating their diverse roles in the development of *H. coronarium*. Based on discoveries of novel miRNAs in *Arabidopsis thaliana* and other species, 90 target genes from 30 miRNAs families were predicted (Table 2). Many of these genes belong to regulatory element families such as GAMYB transcription factors, TCP4 transcription factors, auxin receptor TIR and ARF, scarecrow-like proteins, which regulate the expression of various genes during plant growth, development, and biotic or abiotic stress responses. Among them, hco-miR159 was predicted to target the highest number of genes (10 target genes), reflecting the conservation of hco-miR159. This result is consistent with previous findings in *Lilium davidii* var. *unicolor*, where miR159 is the largest miRNA family [32]. miR159 is an ancient miRNA family, and the diversity among miR159 members may be attributed to gene mutations induced by environmental factors during plant evolution, suggesting that the miR159 family may possess evolutionary diversity [36]. These findings provide valuable insights into the miRNAs of Zingiberaceae plants.

Plant hormones play a crucial role as components of signaling pathways, influencing secondary metabolite synthesis and plant tolerance. In this study, hco-miR167, hco-miR171, and hco-miR393 were

found to target *HcARF8*, *HcSCR15*, and *HcTIR1*, respectively, participating in plant hormone signaling transduction pathways (Table 2). Additionally, the primary volatile aroma compounds of *H. coronarium* are eucalyptol, ocimene, and linalool, with their volatile emissions increasing continuously as the flower opens, peaking during the F5 stage, and slightly declining as the flower ages. Exogenous auxin application plays a crucial role in regulating the synthesis and accumulation of numerous secondary metabolites. In this study, treatment with IAA significantly increased the content of ocimene, eucalyptol, and allo-ocimene in *H. coronarium*, while treatment with PCIB resulted in a significant decrease in the content of ocimene, linalool, allo-ocimene, and methyl benzoate. This suggests that auxin influences the release of floral fragrance compounds in *H. coronarium*, similar to the results of Ke et al. [21].

In plants, ARF genes and TIR genes have been extensively studied, with regulatory modules involving miR167-ARF and miR393-TIR playing crucial roles in processes such as flower development, adventitious root formation, and salt and drought tolerance. Nevertheless, research on the involvement of these two modules in the formation of floral scent remains limited. Studies have revealed that the miR167 family represents a conserved microRNA in plants, primarily regulating genes of the ARF family to influence auxin signaling and modulate various aspects of plant growth and development. Duan et al. [37] investigated miRNA167 in tomatoes, discovering that STTM-miR167a, by elevating the expression levels of *SlARF6* and *SlARF8*, altered the contents of carotenoids and lycopene, thereby delaying fruit ripening and senescence in tomatoes. Gutierrez et al. [38] discovered that in *Arabidopsis*, miR167 targets ARF6 and ARF8, which are involved in the auxin signaling pathway and positively regulate the formation of adventitious roots. Furthermore, miRNA393 is known to modulate the miR156-IPA1-miR408-5p-IAA30 module, thereby participating in auxin signaling transduction in rice [39]. In this study, combining high-throughput miRNA sequencing and degradome sequencing analysis, we identified that the auxin-related genes *HcARF8* and *HcTIR1* in *H. coronarium* are regulated by hco-miR167n and hco-miR393a, respectively (Fig. 6). This finding aligns with previous studies where TIR1 and ARF8 were identified as targets of miR393 and miR167, involved in plant hormone responses [40, 41]. Moreover, the expression of hco-miR167n and hco-miR393a significantly increased after IAA treatment, suggesting these miRNAs may regulate the accumulation of floral fragrance compounds by modulating their respective targets. STTM and VIGS experiments indicated that hco-miR167n and hco-miR393a are positive regulators of floral fragrance metabolism, while *HcARF8* and *HcTIR1* act as negative regulators. Furthermore, downregulation of *HcARF8* and *HcTIR1* by hco-miR167 and hco-miR393 in petals, respectively, regulates the production of terpenoid compounds. These results reveal a novel regulatory mechanism of floral fragrance in *H. coronarium* and provide insights for breeding programs aimed at improving floral fragrance through genetic modification.

H. coronarium, valued for its intense fragrance and vibrant flower colors, is widely utilized in horticultural landscaping and cut flower markets. Its primary aroma constituents are terpenoid compounds, the most diverse class of fragrance compounds characterized by variations in structure and the number of isoprene units, categorizing them into monoterpenes, sesquiterpenes, diterpenes, etc. Terpene synthases (TPS) play a pivotal role at the terminal stage of terpenoid biosynthesis, catalyzing the formation of specific terpenoid compounds from substrates such as GPP, FPP, and GGPP [42]. Some

studies suggest that miRNAs also play a role in regulating plant floral fragrance compounds. miR156 targets SPL genes, and SPL9 directly binds to the promoter of *AtTPS21* to activate its expression, thereby regulating the release of sesquiterpenes during *Arabidopsis thaliana* flower development [43]. However, whether miRNAs in *H. coronarium* target relevant genes to regulate floral fragrance release remains unclear. Therefore, to explore the mechanism of miRNA regulation on floral fragrance, we conducted dual-luciferase and yeast one-hybrid assays on the promoters of *HcARF8* and *HcTPS* genes. The results indicate that *HcARF8* can bind to the promoter of *HcTPS8* and transcriptionally activate its expression, thereby participating in the regulation of terpenoid synthesis in *H. coronarium* (Fig. 9). This study employed high-throughput sequencing technology and molecular biology methods to preliminarily elucidate the regulatory network of miRNAs in *H. coronarium*, targeting key genes to control the release of floral fragrance compounds. Building upon earlier research by our team, this study proposes a regulatory network of miRNAs in *H. coronarium* (Fig. 10). Specifically, hco-miR167 targets and degrades *HcARF8*, which in turn binds to the promoter of *HcTPS8*, thereby transcriptionally inhibiting its expression. Additionally, hco-miR393a targets the auxin receptor *HcTIR1*, indirectly influencing the synthesis of floral fragrance compounds in *H. coronarium*.

Conclusion

This study identified that the volatile emissions of the primary floral fragrance compounds eucalyptol, ocimene, and linalool in *H. coronarium* increase continuously as the flower opens. Across different developmental stages of *H. coronarium*, 171 conserved miRNAs from 24 miRNA families and 32 novel miRNAs were identified using high-throughput sRNA sequencing. Degradome sequencing revealed 102 mRNA degradation sites corresponding to 90 target genes from 30 miRNA families. Exogenous treatments with IAA and the auxin inhibitor PCIB were found to affect the release of floral fragrance compounds in *H. coronarium*. Molecular biology experiments confirmed that hco-miR167n and hco-miR393a act as positive regulators of floral fragrance metabolism in *H. coronarium*, while *HcARF8* and *HcTIR1* act as negative regulators. Specifically, *HcARF8* binds to the promoter of the terpene synthase *HcTPS8*, thereby regulating the synthesis of floral fragrance compounds. In conclusion, this study utilized high-throughput small RNA sequencing for the first time to identify miRNAs in *H. coronarium*, laying the foundation for research on miRNA-mediated regulation of floral fragrance and terpenoid biosynthesis. Furthermore, by modulating miRNAs or their target genes involved in terpenoid compound regulation, it may be possible to enhance the accumulation of these compounds, offering new avenues for improving plant fragrance.

Declarations

Supplementary information

The data presented in the study is included in the article/Supplementary Material.

Authors' contributions

Y.P.F.designed and conceived the experiment. F.W. wrote the paper. F.W. and L.L. carried out the experiments and analyzed the data. R.C.Y. and X.L. conducted the resource survey. X.Y.L.,Y.Y.Y and Y.C.Y. supervised and managed the experiment. Y.P.F. and R.C.Y. revised the manuscript.

Funding

This work was financially supported by the Rural Revitalization Strategy of Guangdong Province(Grant No.2022-NPY-00-042).

Acknowledgments

This work was supported by the Rural Revitalization Strategy of Guangdong Province.

Ethics approval and consent to participate

Not applicable.

Consent for publication

Not applicable.

Competing interests

The authors declare no competing interests.

References

1. Minow, M.A., Coneva, V., Lesy, V., Misyura, M., Colasanti, J., 2022. Plant gene silencing signals move from the phloem to influence gene expression in shoot apical meristems. BMC Plant Biol, 22(1):606.
2. Bai, S., Tian, Y., Tan, C., Bai, S., Hao, J., Hasi, A., 2020. Genome-wide identification of microRNAs involved in the regulation of fruit ripening and climacteric stages in melon (*Cucumis melo*). Hortic Res, 7:106.
3. Moran, Y., Fredman, D., Praher, D., Li, X.Z., Wee, L.M., Rentzsch, F., Zamore, P.D., Technau, U., Seitz, H., 2014. Cnidarian microRNAs frequently regulate targets by cleavage. Genome Res, 24(4):651-663.
4. Tang, Y.Y., Liu, H.H., Guo, S.Y., Wang, B., Li, Z.T., Chong, K., Xu Y.Y., 2017. OsmiR396d Affects Gibberellin and Brassinosteroid Signaling to Regulate Plant Architecture in Rice. Plant Physiol, 176(1):946-959.
5. Cai, J.H., Wu, Z.L., Hao, Y.W., Liu, Y.L., Song, Z.Y., Chen, W.X., Li, X.P., Zhu, X.Y., 2021. Small RNAs, Degradome, and Transcriptome Sequencing Provide Insights into Papaya Fruit Ripening Regulated by 1-MCP. Foods, 10(7):1643.

6. Dai, X.H., Lu, Q., Wang, J., Wang, L.L., Xiang, F.N., Liu, Z.H., 2021. MiR160 and its target genes ARF10, ARF16 and ARF17 modulate hypocotyl elongation in a light, BRZ, or PAC-dependent manner in *Arabidopsis*: miR160 promotes hypocotyl elongation. Plant Sci, 303:110686.
7. Li, J., Wang, Y.Z., Zhang, Y.X., Wang, W.Y., Irish, V.F., Huang, T.B., 2016. RABBIT EARS regulates the transcription of TCP4 during petal development in *Arabidopsis*. J Exp Bot, 67(22):6473-6480.
8. Lian, J.P., Yuan, C., Feng, Y.Z., Liu, Q., Wang, C.Y., Zhou, Y.F., Huang, Q.J., Zhu, Q.F., Zhang, Y.C., Chen, Y.Q., Yu, Y., 2023. MicroRNA397 promotes rice flowering by regulating the photorespiration pathway. Plant Physiol, 194(4):2101-2116.
9. Jerome Jeyakumar, J.M., Ali A., Wang, W.M., Thiruvengadam, M., 2020. Characterizing the role of the miR156-SPL network in plant development and stress response. Plants, 9(9):1206.
10. Millar, A.A., Lohe, A., Wong, G.G., 2019. Biology and function of miR159 in plants. Plants, 8(8):255.
11. Sang, Q., Vayssières, A., Ó'Maoiléidigh, DS., Yang, X., Vincent, C., Bertran Garcia de Olalla, E., Cerise M., Franzen, R., Coupland, G., 2022. MicroRNA172 controls inflorescence meristem size through regulation of APETALA2 in *Arabidopsis*. New Phytol, 235(1):356-371.
12. Baker, C.C., Sieber, P., Wellmer, F., Meyerowitz, E.M., 2005. The early extra petals1 mutant uncovers a role for microRNA miR164c in regulating petal number in *Arabidopsis*. Curr Biol, 15:303-315.
13. Hou, C.Y., Wu, M.T., Lu, S.H., Hsing, Y.I., Chen, H.M., 2014. Beyond cleaved small RNA targets: unraveling the complexity of plant RNA degradome data. BMC Genomic, 15:15.
14. Addo-Quaye, C., Eshoo, T.W., Bartel D.P, Axtell M.J., 2008. Endogenous siRNA and miRNA targets identified by sequencing of the *Arabidopsis* degradome. Curr Biol, 18(10):758-762.
15. Sun, Z.T., He, Y.Q., Li, J.M., Wang, X., Chen, J.P., 2015. Genome-wide characterization of rice black streaked dwarf virus-responsive microRNAs in rice leaves and roots by small RNA and degradome sequencing. Plant Cell Physiol, 56(4):688-699.
16. Zhao, Y.P., Xu, Z.H., Mo, Q.C., Zou, C., Li, W.X., Xu, Y.B., Xie, C.X., 2013. Combined small RNA and degradome sequencing reveals novel miRNAs and their targets in response to low nitrate availability in maize. Ann Bot, 112(3):633-642.
17. Kim, J.E., Park, J.H., Lim, C.J., Lim, J.Y., Ryu, J.Y., Lee, B.W., Choi, J.P., Kim, W.B., Lee, H.Y., Choi, Y.R., 2012. Small RNA and transcriptome deep sequencing proffers insight into floral gene regulation in *Rosa* cultivars. BMC Genomics, 13:657.
18. Jin, Q.J., Xue, Z.Y., Dong, C.L., Wang, Y.J., Chu, L.L., Xu, Y.C., 2015. Identification and characterization of microRNAs from tree peony (*Paeonia ostii*) and their response to copper stress. PLoS One, 10(2):e0117584.
19. Jodder, J., 2020. miRNA-mediated regulation of auxin signaling pathway during plant development and stress responses. J Biosci, 45:91.
20. Iglesias, M.J., Terrile, M.C., Windels, D., Lombardo, M.C., Bartoli, C.G., Vazquez, F., Estelle, M., Casalongué, C.A., 2014. MiR393 regulation of auxin signaling and redox-related components during acclimation to salinity in *Arabidopsis*. PLoS One, 9(9):e107678.

21. Ke, Y.G., Abbas, F., Zhou, Y.W., Yu, R.C., Fan, Y.P., 2021. Auxin-responsive R2R3-MYB transcription factors HcMYB1 and HcMYB2 activate volatile biosynthesis in *Hedychium coronarium* flowers. Front Plant Sci, 12:710826.
22. Yue, Y.C., Yu, R.C., Fan, Y.P., 2014. Characterization of two monoterpene synthases involved in floral scent formation in *Hedychium coronarium*. Planta, 240(4):745-762.
23. Niemeyer, M., Moreno Castillo, E., Ihling, C.H., Iacobucci, C., Wilde, V., Hellmuth, A., Hoehenwarter, W., Samodelov, S.L., Zurbriggen, M.D., Kastritis, P.L., 2020. Flexibility of intrinsically disordered degrons in AUX/IAA proteins reinforces auxin co-receptor assemblies. Nat Commun, 11(1):2277.
24. Wang, C., He, X.W., Wang, X.X., Zhang, S.X., Guo, X.Q., 2017. ghr-miR5272a-mediated regulation of GhMKK6 gene transcription contributes to the immune response in cotton. J Exp Bot, 68(21-22):5895-5906.
25. Djami-Tchatchou, A.T., Sanan-Mishra, N., Ntushelo, K., Dubery, I.A., 2017. Functional roles of microRNAs in agronomically important plants—potential as targets for crop improvement and protection. Front Plant Sci, 8:378.
26. Wu, B., Li, Y., Yan, H.X., Ma, Y.M., Luo, H.M., Yuan, L.C., Chen, S.L., Lu, S.F., 2012. Comprehensive transcriptome analysis reveals novel genes involved in cardiac glycoside biosynthesis and mlncRNAs associated with secondary metabolism and stress response in *Digitalis purpurea*. BMC genomics, 13:1-22.
27. Fan, K., Fan, D.M., Ding, Z.T., Su, Y.H., Wang, X.C., 2015. Cs-miR156 is involved in the nitrogen form regulation of catechins accumulation in tea plant (*Camellia sinensis* L.). Plant Physiol Biochem, 97:350-360.
28. Vashisht, I., Mishra, P., Pal, T., Chanumolu, S., Singh, T.R., Chauhan, R.S., 2015. Mining NGS transcriptomes for miRNAs and dissecting their role in regulating growth, development, and secondary metabolites production in different organs of a medicinal herb, *Picrorhiza kurroa*. Planta, 241(5):1255-1268.
29. Wang, Y.L., Wang, Y.Q., Song, Z.Q., Zhang H.Y., 2016. Repression of MYBL2 by both microRNA858a and HY5 leads to the activation of anthocyanin biosynthetic pathway in *Arabidopsis*. Mol Plant, 9(10):1395-1405.
30. Chen, Y.B., Liao, B.B., Lin, X.H., Luo, Q.S., Huang, X.Y., Wang, X.J., Shan, Q.L., Wang, Y.Q., 2022. Integrative Analysis of miRNAs and Their Targets Involved in Ray Floret Growth in *Gerbera hybrida*. Int J Mol Sci, 23(13):7296.
31. Shi, Y., Xia, H., Cheng, X.T., Zhang, L.B., 2021. Genome-wide miRNA analysis and integrated network for flavonoid biosynthesis in *Osmanthus fragrans*. BMC genomics, 22(1):141.
32. Zhang, J., Yang, Y., Wang, Z.P., Li, X.Y., Sun, H.M., 2021. Evidence of the regulatory roles of candidate miRNAs during somatic embryogenesis in *Lilium davidii* var. *unicolor*. J Plant Growth Regul, 40:197-214.
33. Parreira, J.R., Cappuccio, M., Balestrazzi, A., Fevereiro, P., Araújo, SdS., 2021. MicroRNAs expression dynamics reveal post-transcriptional mechanisms regulating seed development in *Phaseolus*

vulgaris L. Hortic Res, 8(1):18.

34. Roy, S., Tripathi, AM., Yadav, A., Mishra, P., Nautiyal, C.S., 2016. Identification and expression analyses of miRNAs from two contrasting flower color cultivars of canna by deep sequencing. PloS one, 11(1):e0147499.
35. Yang, J.H., Liu, X.Y., Xu, B.C., Zhao, N., Yang, X.D., Zhang, M.F., 2013. Identification of miRNAs and their targets using high-throughput sequencing and degradome analysis in cytoplasmic male-sterile and its maintainer fertile lines of *Brassica juncea*. BMC genomics, 14:1-16.
36. Chen X., Zeng Y., Wang J., Chen X., Xiaoping X., 2017. Evolutionary characteristics of miR159 gene family in *Dimocarpus longan* Lour., and their spatial and temporal expression. Chin J Appl Environ Biol, 23:602-608.
37. Duan, W.H., Yan, J.R., Li, L., Song, H.M., Meng, L.H., Zhang, Z.K., Xu, X.B., Wang, Q., Li J.K., 2024. Silencing Sly-miR167a delayed preharvest ripening of tomato fruit. Postharv Biol Technol, 211:112828.
38. Gutierrez, L., Bussell, J.D., Pacurar, D.I., Schwambach, J., Pacurar, M., Bellini, C., 2009. Phenotypic plasticity of adventitious rooting in *Arabidopsis* is controlled by complex regulation of AUXIN RESPONSE FACTOR transcripts and microRNA abundance. Plant Cell, 21(10):3119-3132.
39. Rong, F.X., Lv, Y.S., Deng, P.C., Wu, X., Zhang, Y.Q., Yue, E.K., Shen, Y.X., Muhammad, S., Ni, F.R., Bian, H.W., Wei, X.J., Zhou, W.J., Hu, P.S.,Wu, L., 2024. Switching action modes of miR408-5p mediates auxin signaling in rice. Nat Commun, 15(1):2525.
40. Chen, J., Pan, A., He, S.J., Su, P., Yuan, X.L., Zhu S.W., Liu Z., 2020. Different microRNA families involved in regulating high temperature stress response during cotton (*Gossypium hirsutum* L.) anther development. Int J Mol Sci, 21(4):1280.
41. Zhou, R., Yu, X.Q., Ottosen, C.O., Zhang, T.L., Wu, Z., Zhao, T.M., 2020. Unique miRNAs and their targets in tomato leaf responding to combined drought and heat stress. BMC Plant Biol, 20(1):107.
42. Han, X., Zhang, J.H., Han, S., Chong, S.L., Meng, G.L., Song, M.Y., Wang, Y., Zhou, S.C., Liu, C.C., Lou, L.H., 2022. The chromosome-scale genome of *Phoebe bournei* reveals contrasting fates of terpene synthase (TPS)-a and TPS-b subfamilies. Plant Commun, 3(6):100410.
43. Yu, H., Sole,r M., San Clemente, H., Mila, I., Paiva, J.A., Myburg, A.A., Bouzayen, M., Grima-Pettenati, J., Cassan-Wang, H., 2015. Comprehensive genome-wide analysis of the Aux/IAA gene family in Eucalyptus: evidence for the role of EgrIAA4 in wood formation. Plant Cell Physiol, 56(4):700-714.

Figures

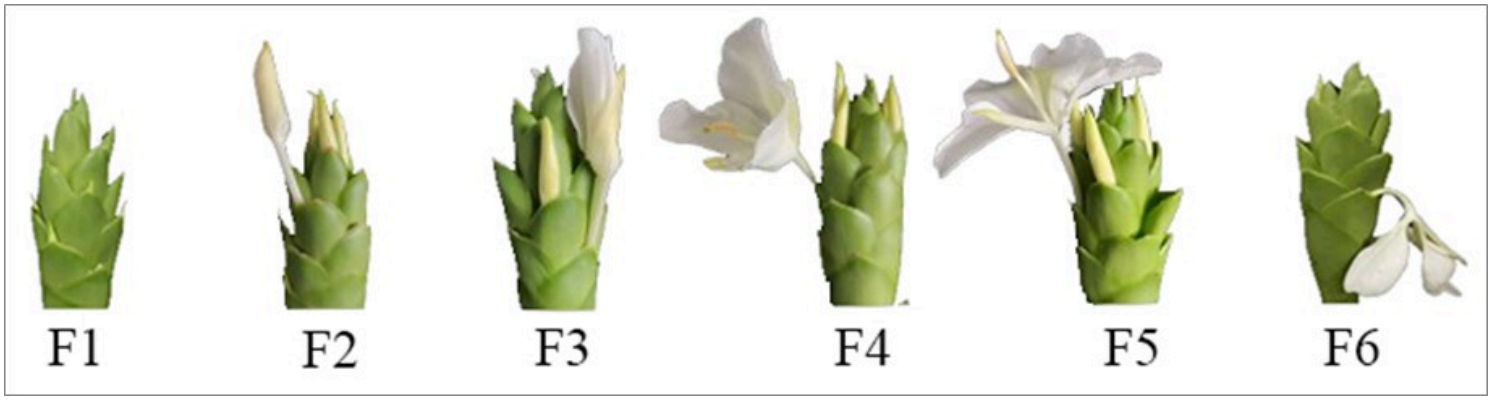

Figure 1

Photographs of *H. coronarium* petals at different developmental stages

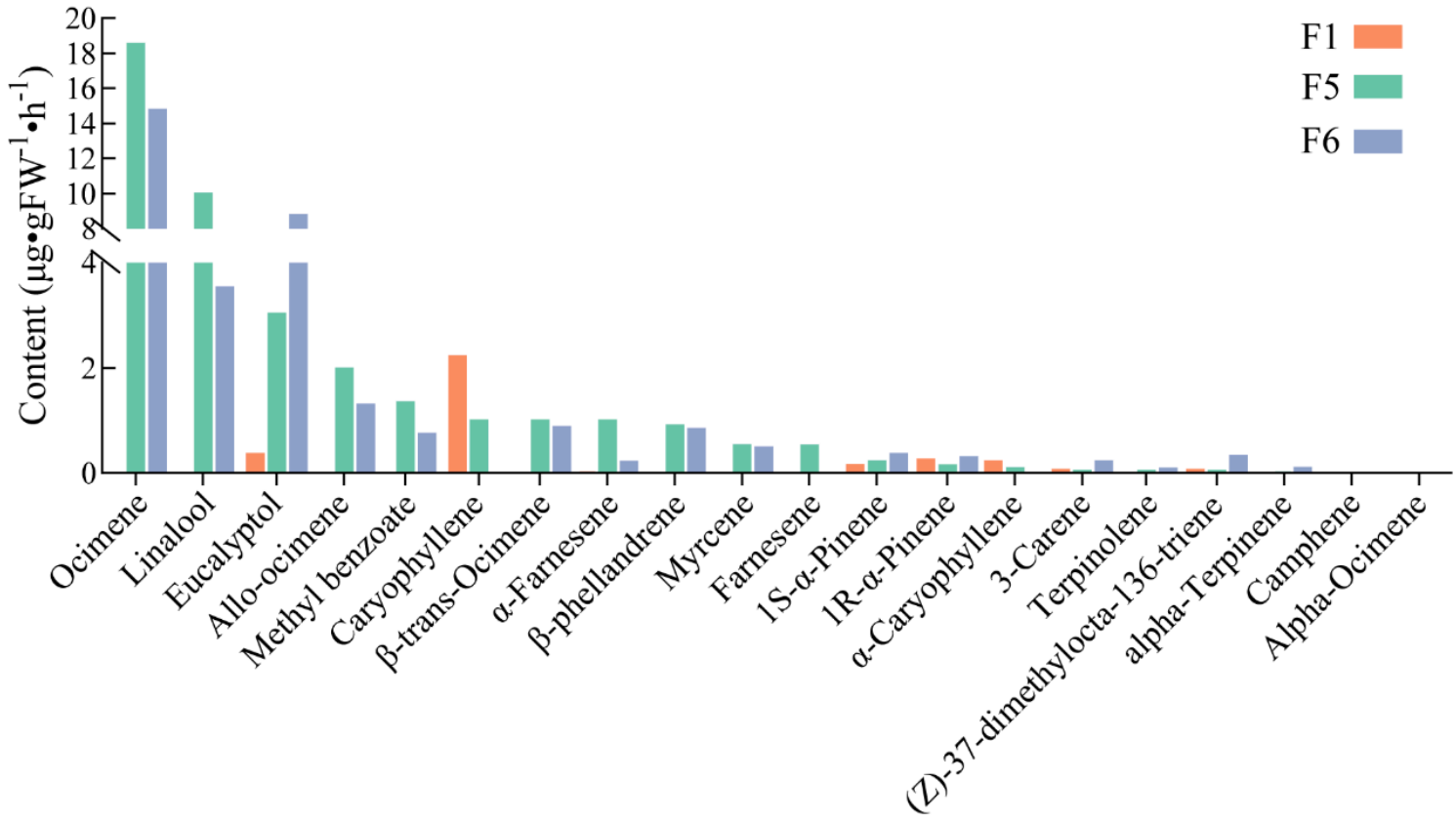

Figure 2

Changes in volatile aroma compounds during different stages in *H. coronarium*

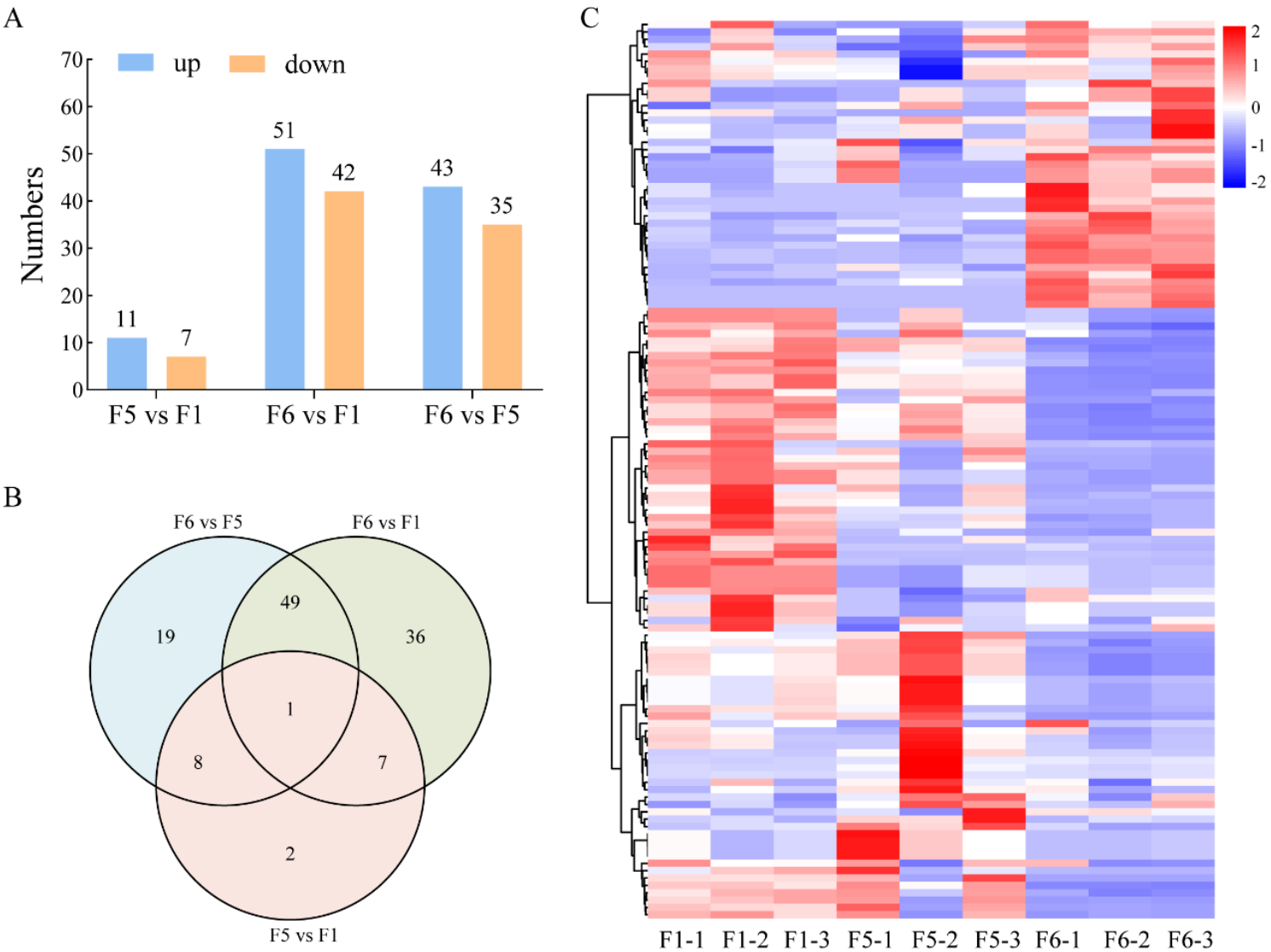

Figure 3

Expression profile of differentially expressed miRNAs in *H. coronarium.* A, The number of differentially expressed miRNAs; B, Venn diagram of differentially expressed miRNAs; C, Expression profile of differentially expressed miRNAs.

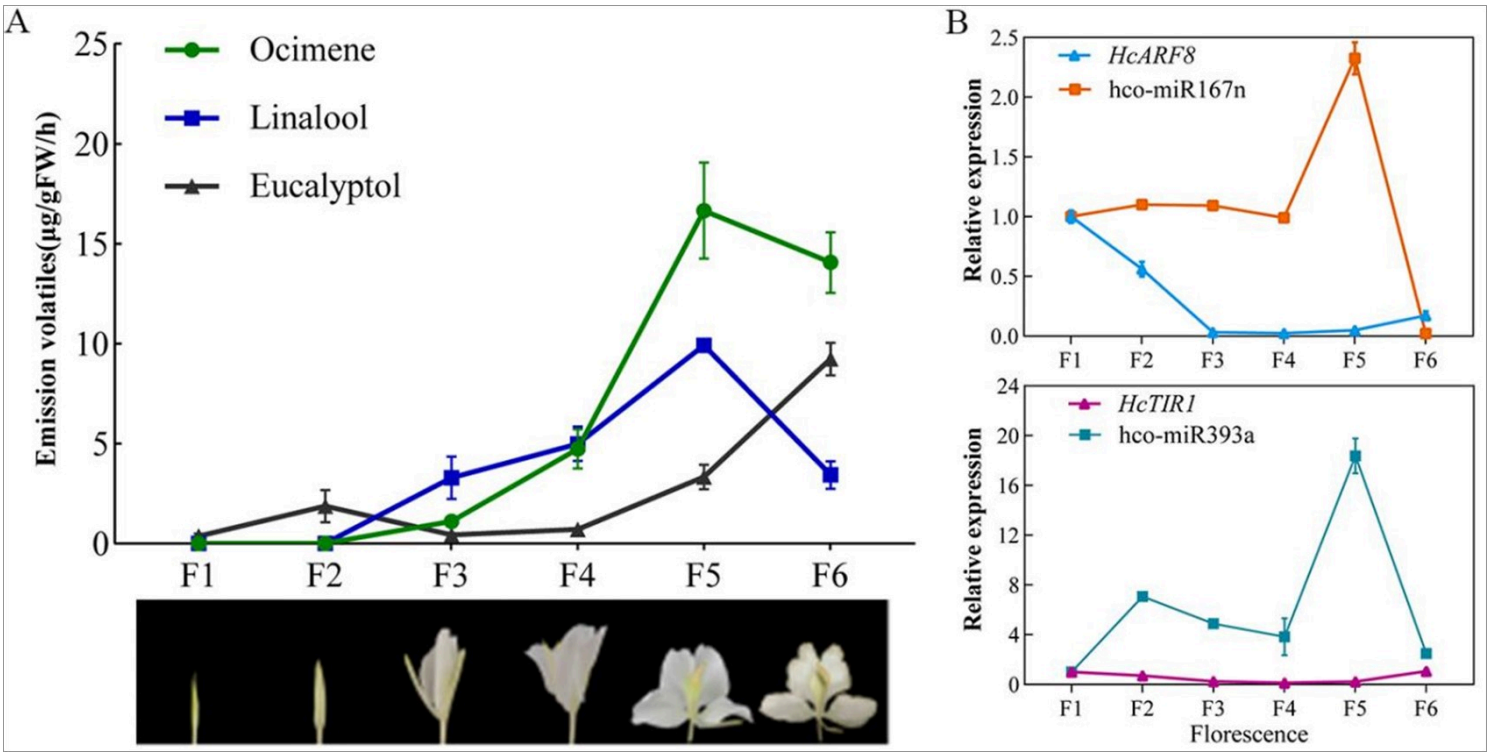

Figure 4

Dynamics of volatile aroma compounds and the relative expression of *HcARF8*-miR167n and *HcTIR1*-miR393a

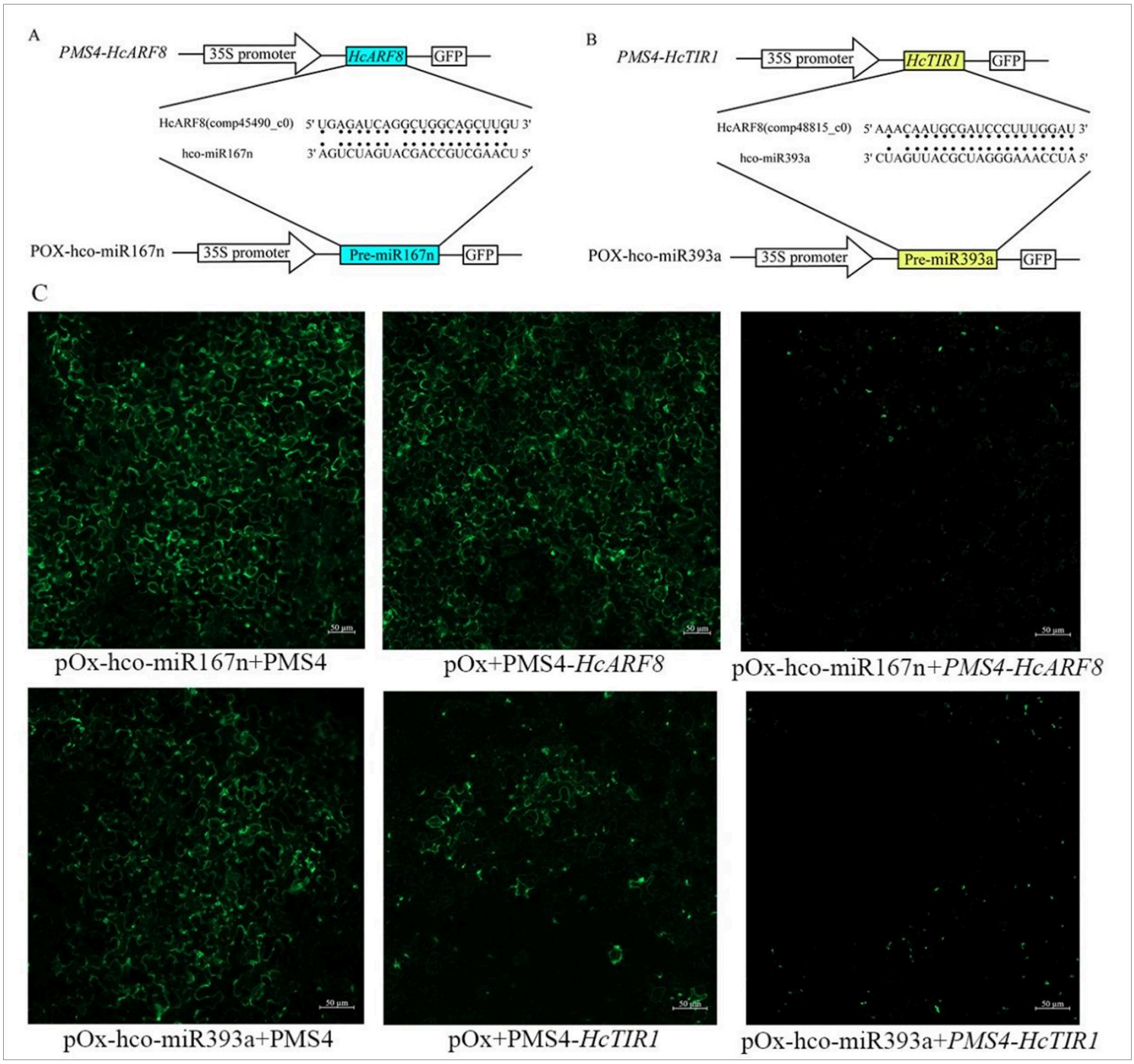

Figure 5

Tobacco co-transformation assay to validate the targeting of *HcARF8* by miR167n and *HcTIR1* by miR393a. A, Schematic diagram of the *PMS4-HcARF8* and pOx-hco-miR167n construct for vector assembly. B, Schematic diagram of the *PMS4- HcTIR1*and pOx-hco- miR393a construct for vector assembly. C, Fluorescence images of each group.

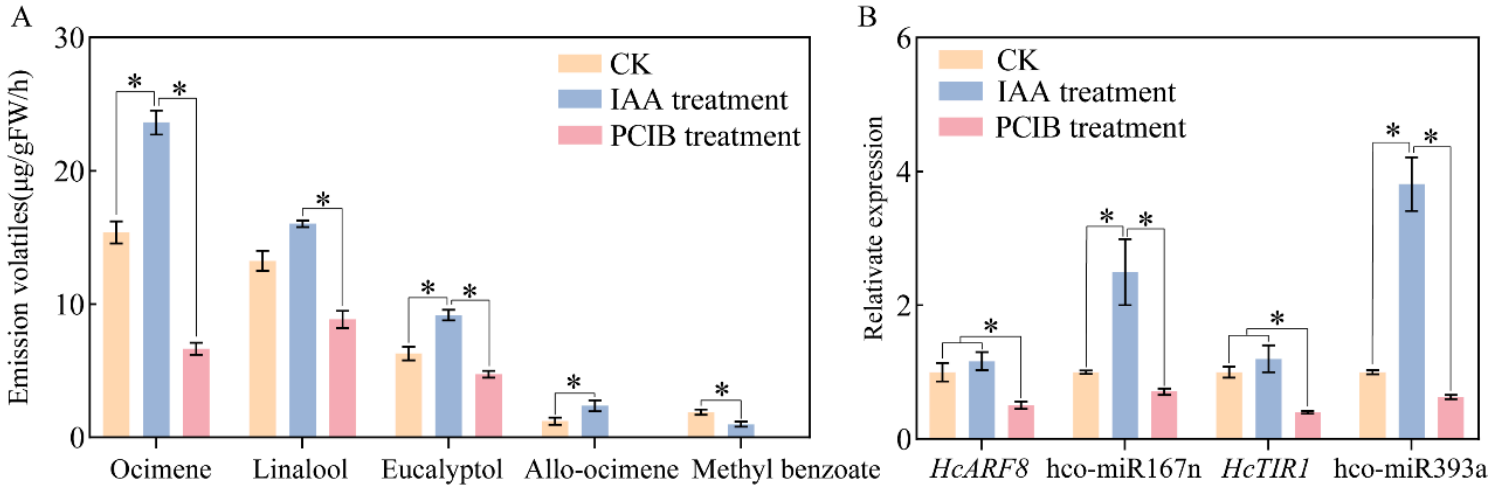

Figure 6

Aroma volatilization and related gene expression after exogenous IAA and PCIB treatment. * P value < 0.05 (Student's t-test)

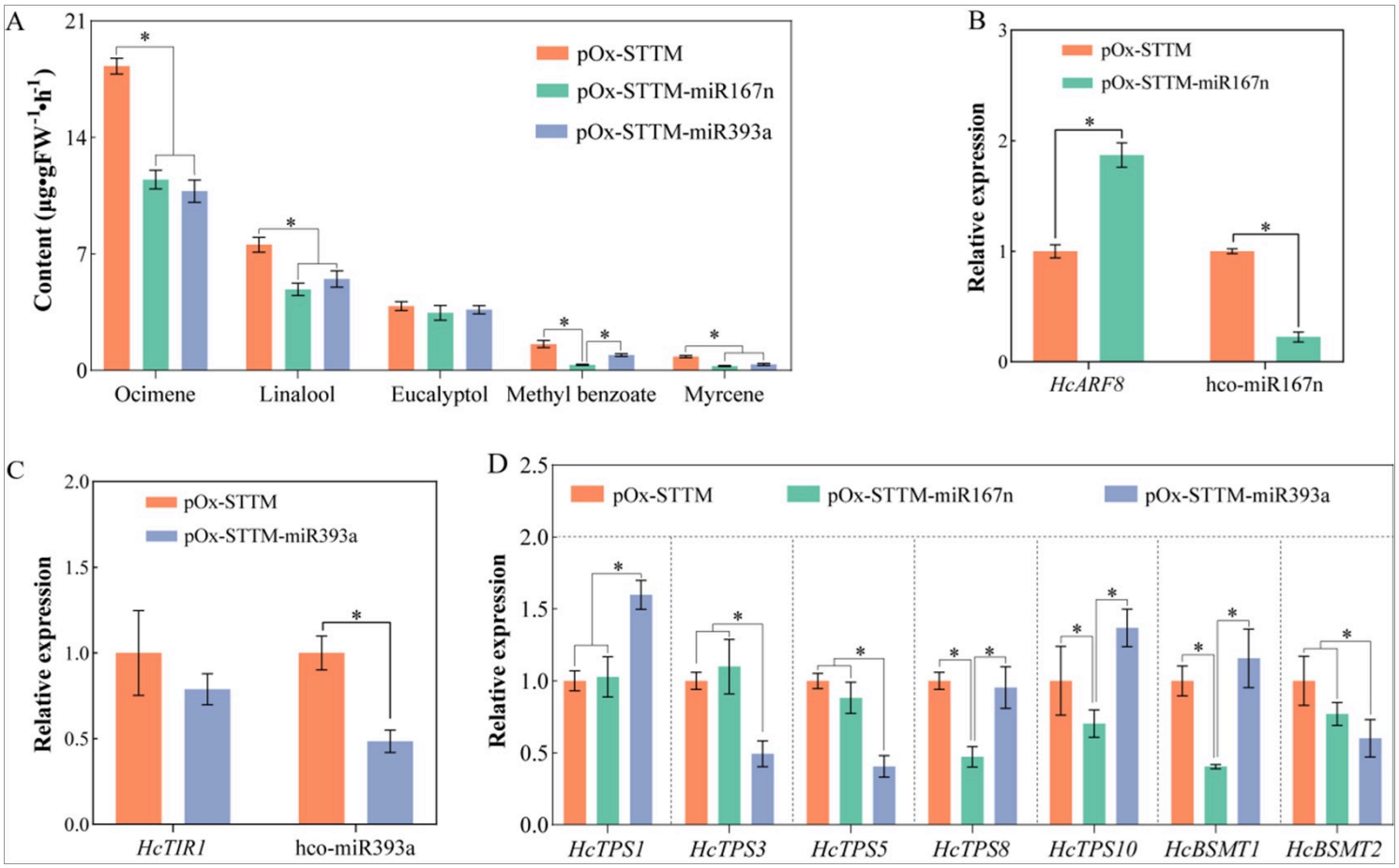

Figure 7

STTM interfered with aroma volatilization and related gene expression after hco-miR167n and hco-miR393a

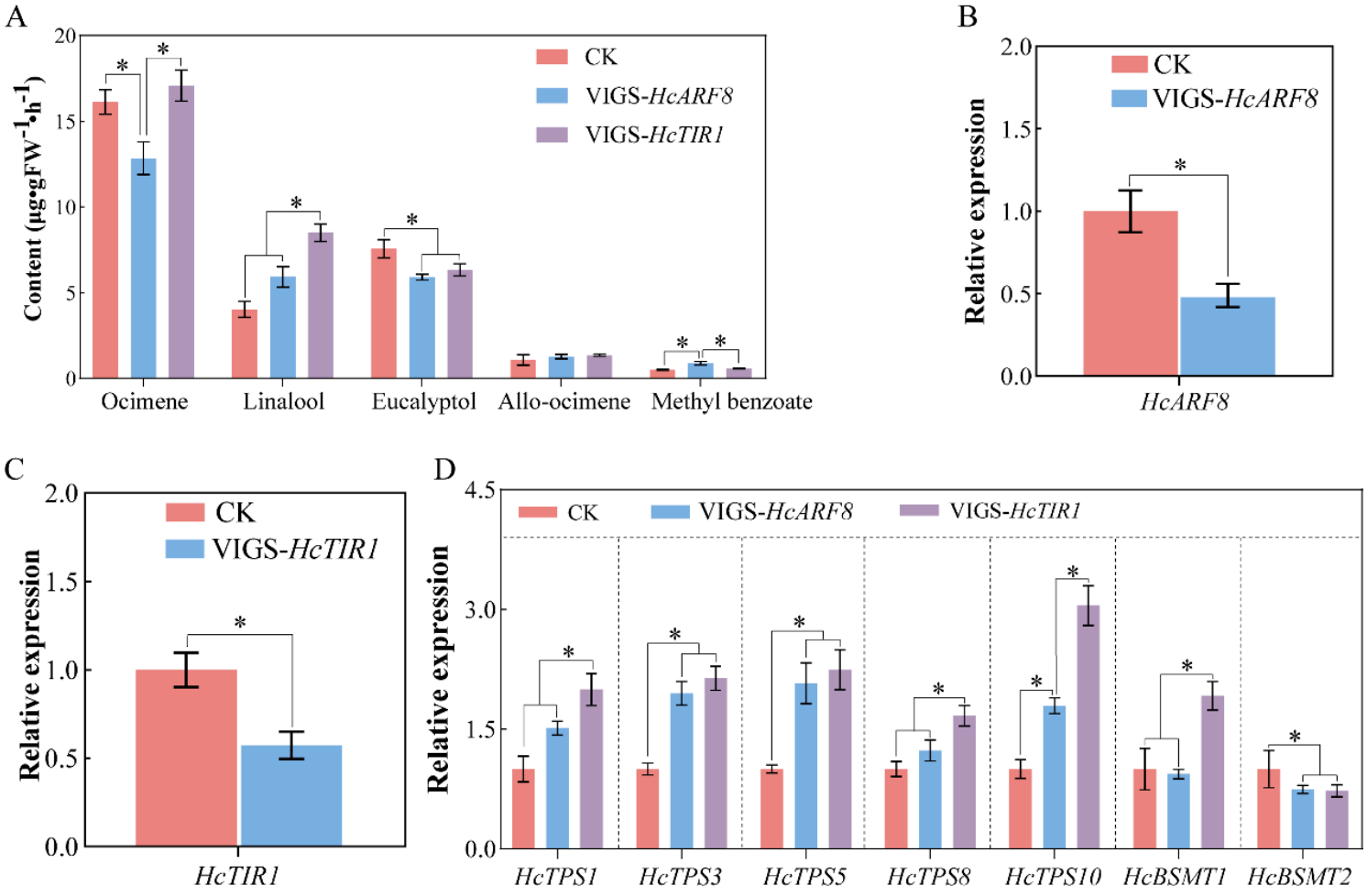

Figure 8

Aroma volatilization and related gene expression after VIGS *HcARF8* and *HcTIR1*

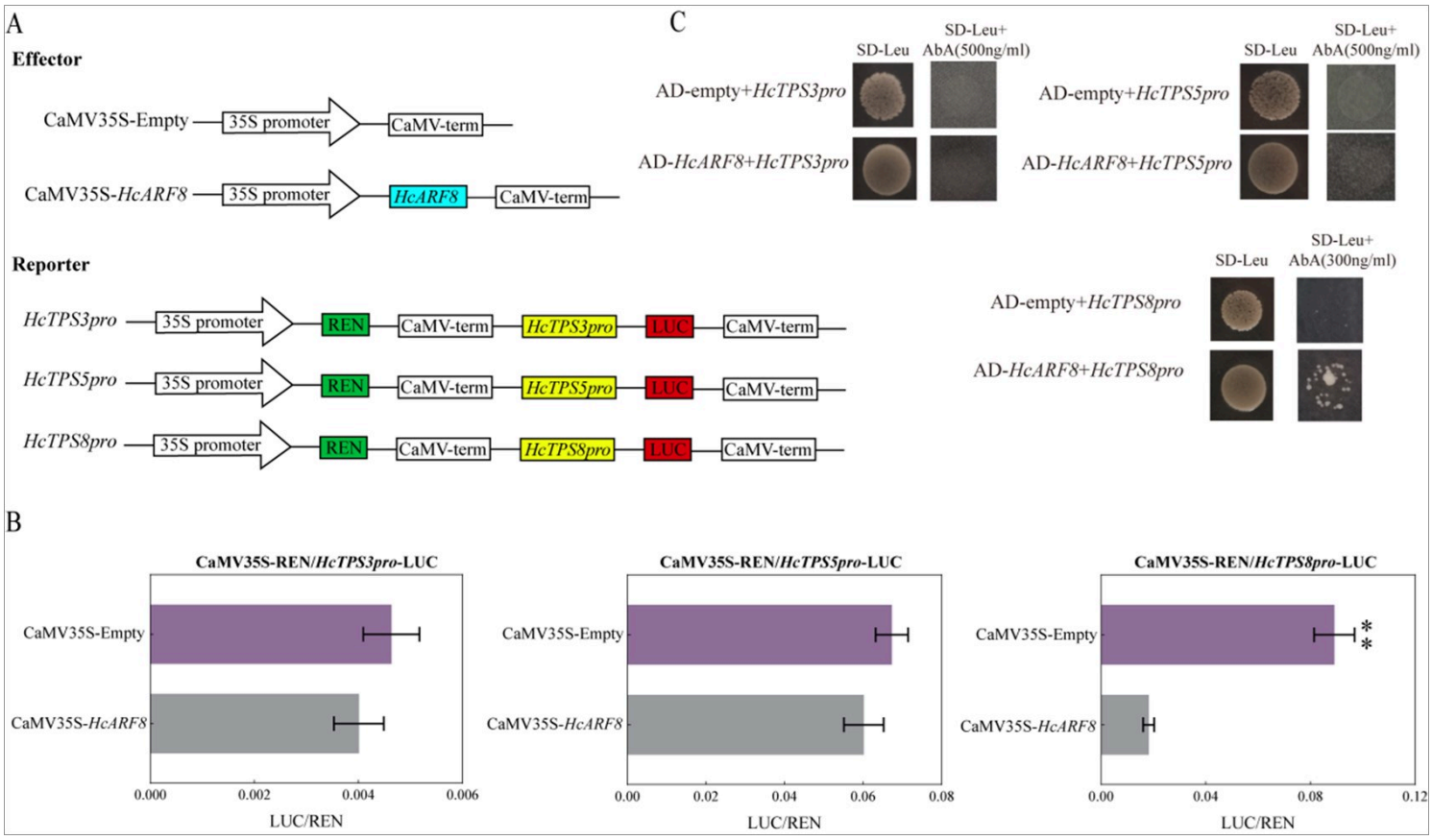

Figure 9

*HcARF8*specifically targets the *HcTPS8* promoter. A, Diagrams of the reporter and effector constructs used for the dual-LUC transient expression assay; B, LUC assay showing the activation of the *HcTPS3/5/8* promoters by *HcARF8*. The LUC/REN ratio reflects transactivation activity. Data are presented as the mean ± SD (n = 3). ** $P < 0.01$; C, Y1H analysis of *HcARF8* binding to the *HcTPS3/5/8* promoter.

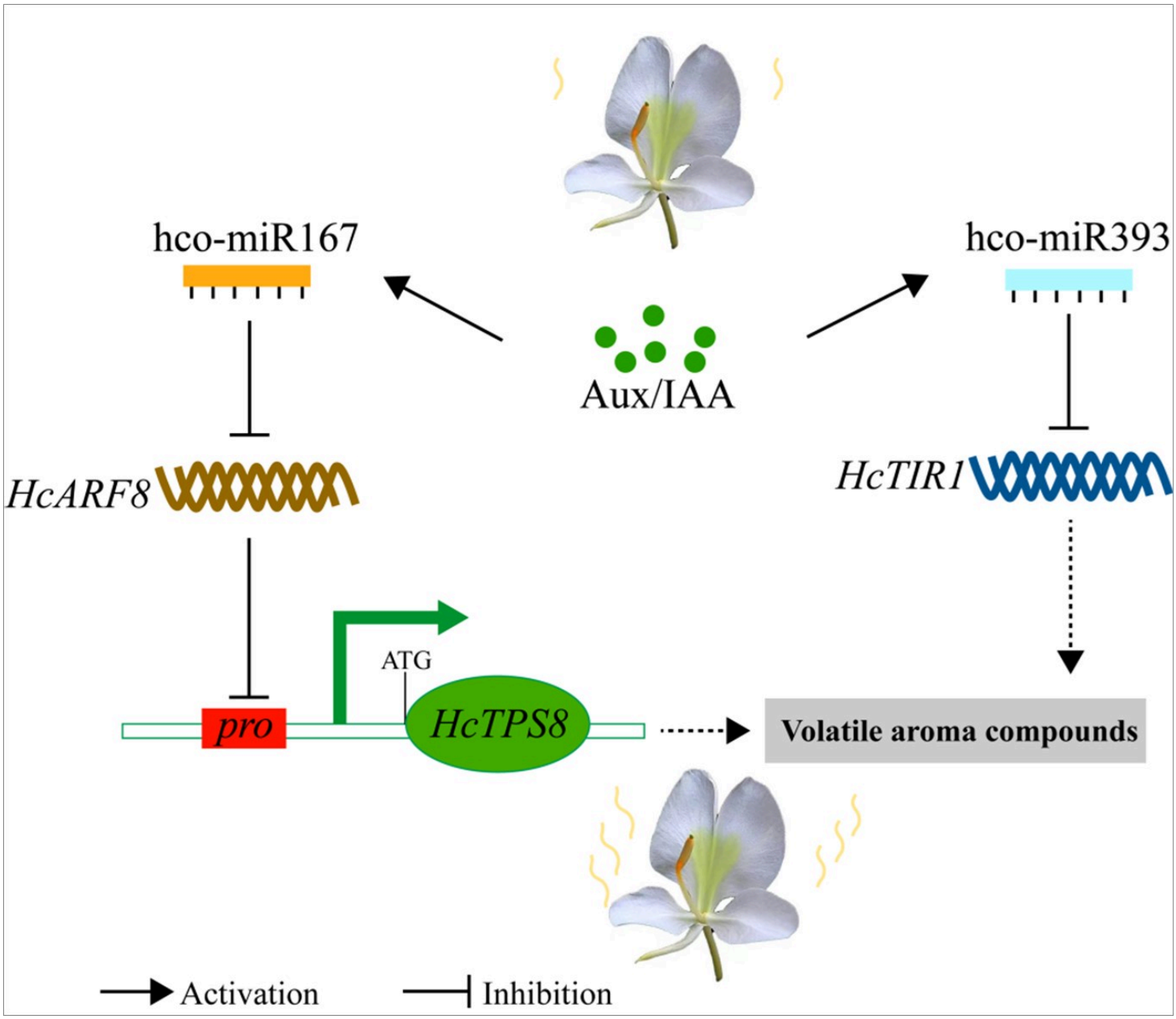

Figure 10

The regulatory network diagram of *HcARF8*-miR167n and *HcTIR1*-miR393a regulating the synthesis of volatile aroma compounds in *H. coronarium*

Supplementary Files

This is a list of supplementary files associated with this preprint. Click to download.

- SupplementaryFigures.docx
- SupplementaryTables.xlsx